2.03 The Dynamics of Strongly Stratified Estuaries

WR Geyer and DK Ralston, Woods Hole Oceanographic Institution, Woods Hole, MA, USA

Glossary

Fjord A long, narrow, and usually deep inlet, often with one or more sills. If there is significant freshwater inflow, the fjord will typically be strongly stratified.

Salt wedge An estuary at the mouth of a river with substantial freshwater inflow, in which there is a strong gradient between nearly freshwater and seawater. The interface between the freshwater and saltwater tilts downward toward land, giving it the approximate form of a wedge.

Shear instability A wavelike disturbance in a vertically sheared flow that causes mixing between the upper and lower layers of fluid.

Stratification A vertical gradient in salinity or density. Stratification is normally stable, that is, heavier fluid lies below lighter fluid, and this stability inhibits vertical mixing.

Subcritical flow In hydraulics, a flow in which the fluid velocity is slower than some critical velocity as defined by the Froude number.

Supercritical flow In hydraulics, a flow in which the fluid velocity is faster than some critical velocity.

Abstract

This chapter examines the dynamics of strongly stratified estuaries by addressing the parameters that lead to strong stratification and by examining the dynamics of different types of strongly stratified estuaries, notably salt wedge estuaries and fjords. Stratification is shown to be determined by the balance between the stratifying tendency of the estuarine circulation and mixing by the tides. Several parametrizations are presented that can be used to estimate the strength of estuarine stratification. The dynamics of highly stratified estuaries are best expressed using the two-layer equations of motion, which are presented in detail in this chapter. The chapter includes a brief discussion of two-layer hydraulic phenomena such as hydraulic transitions, subcritical and supercritical flow. Frictional two-layer processes are discussed both in context with salt wedges and fjords. Discussion of fjord dynamics includes Knudsen's relation expressing the relationship between the strength of the exchange flow, the freshwater inflow, and the salinity difference between the upper and lower layers. Fjord mixing and the concept of overmixing are also discussed.

2.03.1 Introduction

Stratification is one of the most important characteristics of estuaries. It exerts a dominant control on vertical mixing, which profoundly affects the physics and the vertical distribution of chemicals and biota within estuaries. Stratification arises due to the input of freshwater into saline embayments, wherein the influence of gravity causes the freshwater to override the saltwater, separated by a strong halocline. Temperature variations can also cause stratification, but the contribution of salinity almost always dominates in estuarine environments. The input of freshwater into a saline environment is not a sufficient condition to generate a highly stratified estuary; the rate of freshwater input must exceed the mixing rate, which is normally a function of the tidal forcing. Thus, the highly stratified condition may arise due either to particularly strong freshwater inflow or to particularly weak tidal mixing, or some intermediate level of forcing wherein the freshwater input can keep pace against mixing to maintain the stratification.

The parametrization of the conditions that determine estuarine stratification is one of the most interesting and well-trodden aspects of estuarine dynamics, yet there is still no consensus on the key parameters that may predict stratification. The uncertainty arises, in part, because of the diversity of estuarine regimes as well as the variability of conditions within one estuary, both in space and in time. Once this variability is properly addressed, some of the apparent inconsistencies among parametrizations are resolved.

In common classification of estuaries (e.g., Hansen and Rattray, 1966), highly stratified estuaries are of two types: salt wedges and fjords (**Figure 1**). Salt wedges are found at the mouths of rivers, in which the strength of the freshwater outflow overcomes the mixing due to the tides to maintain strong stratification conditions. Salt wedges were originally associated with weak tidal conditions, but more recent research has revealed that high stratification conditions may occur in the presence of intense tidal forcing, as long as the freshwater outflow is adequate to renew the stratification in every tidal cycle.

Fjords are very deep estuaries, usually carved by glaciers, and often with shallow sills separating them from the ocean and dividing them into sub-basins. Fjords, unlike salt wedges, do not always exhibit large vertical salinity differences (e.g., Puget Sound; **Figure 1(b)**). However, they almost always behave dynamically as highly stratified estuaries, due to the relative ineffectiveness of tidal mixing compared to the influence of density variations. This apparent paradox is explained in Section 2.03.2. Another noteworthy feature of fjords is the presence of sills, which are often the sites of intense interaction between the stratified flow and the tidal motion. These interactions lead to internal waves, hydraulic jumps, bores, and shear instabilities.

Stratification has particular significance for estuarine dynamics, due to its dominant influence on vertical mixing. The presence of stratification may reduce the intensity of vertical mixing 100-fold relative to an unstratified water body with the same tidal velocity. This reduction in the intensity of vertical mixing results in much stronger vertical shears than in weakly stratified estuaries; it is common for the velocity difference between surface and bottom waters to exceed $1\,m\,s^{-1}$ in highly stratified estuaries. Vertical mixing of salt is likewise reduced, which results in a positive feedback loop in which the presence of stratification promotes the maintenance and intensification of the stratification (e.g., Simpson et al., 1990). Although mixing is suppressed by stratification, mixing within the pycnocline is an essentially important phenomenon in highly stratified estuaries, whether it occurs near a sill in a fjord or within a tidally forced salt wedge. In fact, some of the most intense mixing observed in the ocean occurs in highly stratified estuaries, specifically because of the intense shears that develop in the presence of strong stratification (MacDonald and Geyer, 2004).

The strong salinity gradient has important consequences for estuarine ecology and water quality. The pycnocline and longitudinal density fronts in a highly stratified estuary divide two very different environments, not only with contrasting salinity but often with different temperature, turbidity, turbulence intensity, and direction of flow. The pycnocline and density fronts provide microhabitats that often result in intense

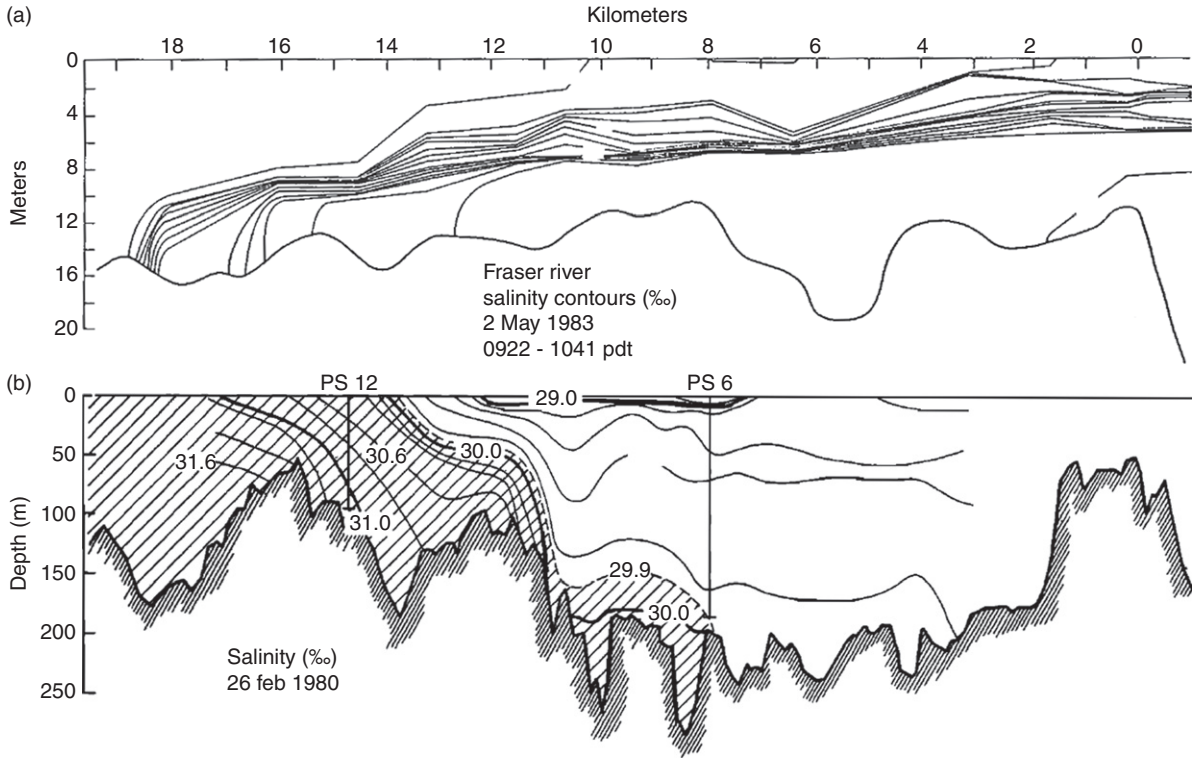

Figure 1 Salinity cross sections in highly stratified estuaries: (a) the Fraser River (Geyer and Farmer, 1989), a salt wedge and (b) Puget Sound (Geyer and Cannon, 1982) – a fjord estuary. Although the top-to-bottom salinity difference in Puget Sound is only 1 psu, it still behaves as a highly stratified estuary, due to the strong influence of stratification in very deep estuaries.

accumulations of organisms (Dekshenieks et al., 2001). In fjords and micro-tidal salt wedges, the long residence time of the underlying saltwater may lead to hypoxic or anoxic conditions. In these systems, the physical mechanisms of bottom water renewal are of particular importance for water quality and ecology.

This chapter examines the dynamics of highly stratified estuaries, first by addressing the parameters that lead to high stratification, then by examining the dynamics of different types of highly stratified estuaries. The chapter concludes with a discussion of the key unresolved questions.

2.03.2 Parameters Controlling Estuarine Stratification

Estuarine stratification is usually defined by the salinity difference Δs between near-surface and near-bottom waters. The relevant dynamical variable is the density difference $\Delta\rho$, which can be related to Δs via the relation

$$\frac{\Delta\rho}{\rho_0} = \beta\Delta s \qquad [1]$$

where $\beta \cong 0.8 \times 10^{-3}\,\text{psu}^{-1}$ (salinity is presented in practical salinity units, roughly equivalent to parts per thousand mass ratio of salt). Temperature also contributes to stratification, although a 1 °C change in temperature is equivalent to 0.2 psu change in salinity, so a thermally stratified estuary cannot attain the same magnitude of vertical density difference as a large vertical salinity difference (e.g., Δs of 10 psu or more).

A number of early investigators of estuarine dynamics noted that the stratification could be predicted based on the ratio of the river flow to the tidal flow, originally stated as the volume of river water entering in one tidal cycle compared to the tidal prism (Schultz and Simmons, 1957). Hansen and Rattray (1966) called this the 'flow ratio' defined as

$$P = \frac{u_f}{u_t} \qquad [2]$$

where $u_f = Q_f/A$, the freshwater discharge rate per unit cross-sectional area of the estuary, and u_t is a representative tidal velocity. According to Schultz and Simmons as well as Hansen and Rattray, a value of $P \sim 0.3$ should lead to highly stratified conditions.

Hansen and Rattray developed a two-dimensional (2D) estuarine classification scheme based on a theoretical examination of estuarine dynamics (**Figure 2**), with stratification (represented as the ratio of the vertical salinity difference to the mean salinity) being one of the dimensions and the estuarine circulation being the other. The purpose of this approach was to illustrate the multidimensional nature of the estuarine regime and to relate the stratification and circulation to readily observed quantities such as P and the freshwater Froude number

$$F_m = \frac{u_f}{u_d} \qquad [3]$$

where $u_d = (\beta g s_0 h_0)^{1/2}$ is the densimetric velocity (where g the acceleration of gravity, s_0 the oceanic salinity, and h_0 the water depth). This is the maximum possible velocity that can be driven by the density gradient within the estuary. According to the semi-empirical analysis by Hansen and Rattray, the stratification depends not just on P but on $P^2/F_m = u_f u_d/u_t^2$. This indicates a more sensitive dependence on tidal mixing than on the buoyancy input by the river flow.

Fischer (1972) reanalyzed the data presented by Hansen and Rattray (1966) and used energy arguments to obtain an improved parametrization for stratification called the estuarine Richardson number

$$Ri_e = \frac{\beta g s_0 h_0 u_f}{u_t^3} = \frac{u_d^2 u_f}{u_t^3} \qquad [4]$$

The numerator represents the potential energy input due to the river inflow and the denominator is proportional to the work done by bottom stress. When Ri_e exceeds 1 or so, highly stratified conditions should occur in an estuary.

A limitation of Fischer's approach is that it does not consider the horizontal scale of the estuary, or more precisely the aspect ratio of length to depth. Stacey et al. (2001) defined the 'horizontal Richardson number', now called the 'Simpson number'

$$Si = \frac{\beta g\, \partial s/\partial x\, h_0^2}{C_D u_t^2} \qquad [5]$$

where $\partial s/\partial x$ is the along-estuary salinity gradient and C_D is the bottom drag coefficient. This provides a more precise means of defining the ratio of potential energy input to mixing, taking into account the horizontal scale of salinity variation (or, in essence, the length of the estuary). Bowen (2000) showed that this quantity is proportional to $Ri_e^{1/3}$ for partially mixed estuaries in dynamical equilibrium (based on the analytical framework of Chatwin (1976)). It is not known how well this relationship extends to highly stratified estuaries. Either Si or Ri_e may be effective for diagnosing the stratification. In practice, it is often difficult to obtain an estimate of $\partial s/\partial x$, so Ri_e is a more accessible, albeit less precise means of defining the transition to highly stratified conditions.

The first of these two types of highly stratified estuaries, salt wedges, owe their strong stratification to the large value of freshwater outflow velocity u_f, which should be in the range of 15–30% of the tidal velocity for highly stratified conditions to occur (Geyer and Farmer, 1989). In microtidal salt wedges (e.g., the Ebro estuary in Spain), high stratification conditions may occur with fairly weak freshwater outflow, due to small tidal velocities. In macrotidal salt wedges like the Fraser River, high stratification can only occur with high river outflow velocities. Fjords, the second major type of highly stratified estuaries, owe their high stratification to their large depth, which reduces the effectiveness of tidal mixing both by reducing tidal velocities (as the tidal velocity varies inversely with depth for a given tidal prism) and by increasing the potential energy associated with stratification. Both types of estuaries have a distinct pycnocline, often well separated from the bottom boundary layer. In fjords, the pycnocline tends to be very close to the water surface, with the lower layer much thicker than the upper layer, whereas in salt wedges, the upper and lower layers are of comparable thickness. The similar two-layer structure of fjords and salt wedges yields dynamically similar interfacial waves, shear instability, and internal hydraulic transitions.

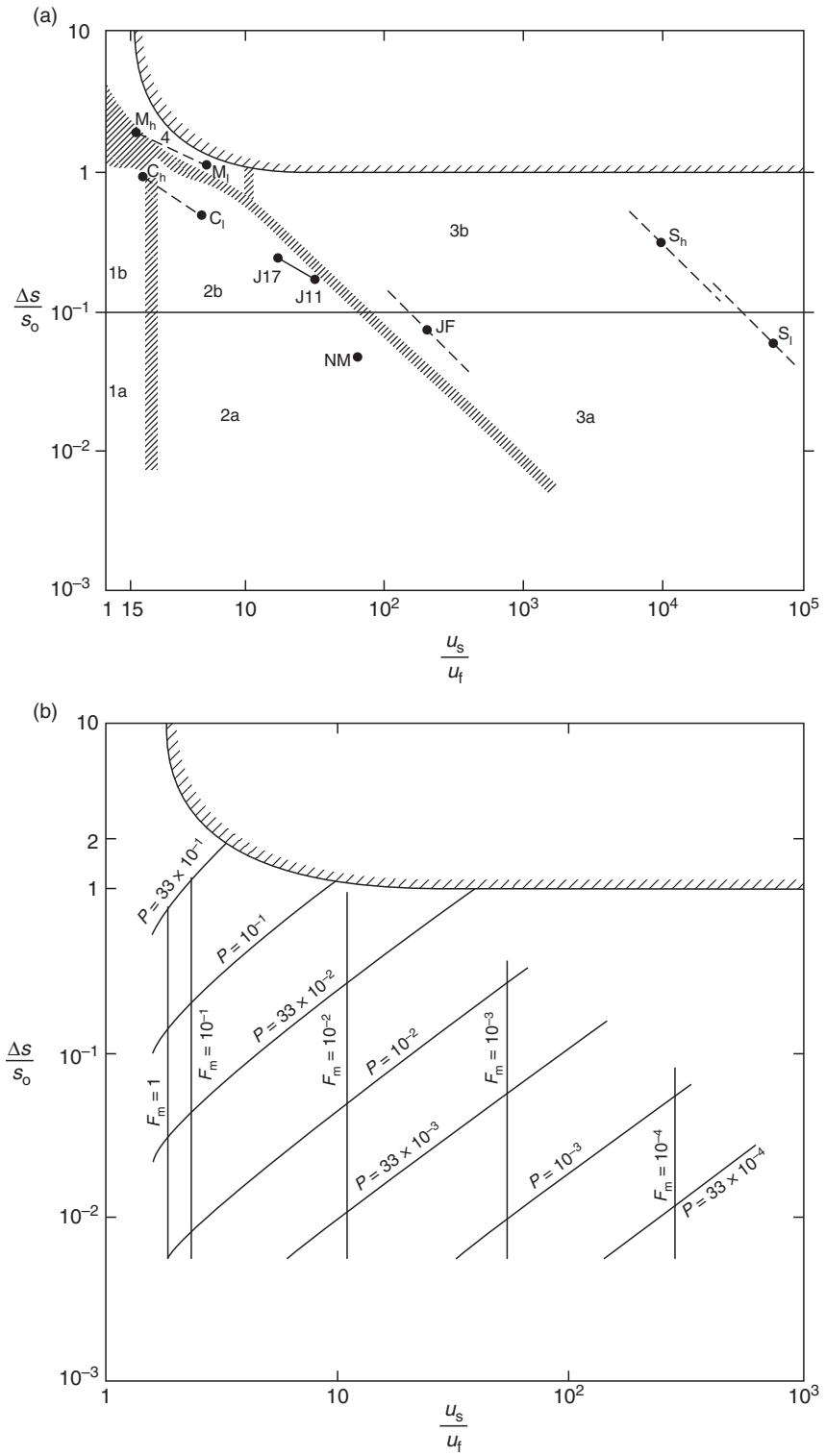

Figure 2 Hansen and Rattray's (1966) estuarine classification diagram. The strength of stratification is represented on the vertical axis as vertical salinity difference normalized by the mean salinity. The horizontal axis represents the strength of the estuarine circulation as represented by the near-surface velocity u_s, normalized by freshwater flow. (a) the position of different estuarine types: salt wedge estuaries (type 4) are found in the upper left part of the diagram, whereas fjords (type. 3a and 3b) are in the far right. Partially mixed (1b and 2b) and well-mixed estuaries (1a and 2a) are found to the left and below the highly stratified estuaries. (b) how the flow ratio P and the freshwater Froude number F_m vary in this parameter space.

Some fjords, such as Puget Sound, have modest vertical salinity gradients, but they still share the dynamics of highly stratified estuaries due to the large potential energy associated with the stratification relative to their kinetic energy. An effective way of quantifying the stratification is via the potential energy anomaly (e.g., Simpson et al., 1990)

$$\Phi = \beta g \int [\bar{s} - s(z)] z \, dz \qquad [6]$$

The parameter Φ represents the energy required to mix the entire water column. Note that this quantity varies as the square of the depth, so deep estuaries are much more resistant to mixing than shallow ones, even with relatively modest vertical salinity contrast.

2.03.3 The Two-Layer Equations

A key simplifying assumption for representing the dynamics of highly stratified estuaries is to divide the estuary into an upper and lower layer separated by the pycnocline. This approach is based on the assumption that exchange between layers is slow compared to advective processes within each layer. Schijf and Schonfeld (1953) provided a particularly clear presentation of these dynamics, also developed by Stommel and Farmer (1952), Keulegan (1957) and more recently by Armi (1985) and Armi and Farmer (1986).

A schematic of the two-layer structure is shown in **Figure 3**. The velocities and salinities (or densities) are assumed to be uniform in each layer, and the pycnocline is treated as an interface of zero thickness. The continuity equation is written as

$$B\frac{\partial h_1}{\partial t} + \frac{\partial Q_1}{\partial x} = 0 \qquad [7a]$$

$$B\frac{\partial h_2}{\partial t} + \frac{\partial Q_2}{\partial x} = 0 \qquad [7b]$$

where h_1 and h_2 are the thicknesses of the upper and lower layer, B is the width of the estuary at the depth of the pycnocline, and Q_1 and Q_2 are the volume transports. Note that the entrainment rate (volume flux between layers) is assumed to be zero here, but that condition can be relaxed for cases in which entrainment is important. The momentum equations can be written most simply in terms of the layer-averaged velocities u_1 and u_2 (assuming that density variations between layers are small compared to the density of either layer, i.e., the Boussinesq approximation):

$$\frac{\partial u_1}{\partial t} + u_1\frac{\partial u_1}{\partial x} + g\frac{\partial \eta}{\partial x} + \frac{C_i|u_1 - u_2|(u_1 - u_2)}{h_1} = 0 \qquad [8a]$$

$$\frac{\partial u_2}{\partial t} + u_2\frac{\partial u_2}{\partial x} + g\frac{\partial \eta}{\partial x} + g'\frac{\partial h_i}{\partial x} - \frac{C_i|u_1 - u_2|(u_1 - u_2)}{h_2} + \frac{C_D|u_2|u_2}{h_2} = 0 \qquad [8b]$$

where $g' = \beta g \Delta s$ is the reduced gravity, $\partial\eta/\partial x$ is the slope of the free surface, $\partial h_i/\partial x$ is the slope of the interface, and C_i is an interfacial drag coefficient. These equations represent both barotropic (e.g., tidal wave propagation) as well as baroclinic processes (e.g., internal waves). The baroclinic dynamics are expressed by taking the difference of the two momentum equations, which eliminates the dependence on the surface pressure gradient

$$\frac{\partial}{\partial t}(u_2 - u_1) + u_2\frac{\partial u_2}{\partial x} - u_1\frac{\partial u_1}{\partial x} + g'\frac{\partial h_i}{\partial x} - C_i|u_1 - u_2|(u_1 - u_2)\left(\frac{1}{h_1} + \frac{1}{h_2}\right) + \frac{C_D|u_2|u_2}{h_2} = 0 \qquad [9]$$

If we assume that the variations in free surface height are small compared with variations in bottom depth, we obtain

$$\frac{\partial h_i}{\partial x} = \frac{\partial h_b}{\partial x} + \frac{\partial h_2}{\partial x} \cong \frac{-\partial h_1}{\partial x} \qquad [10]$$

The advective terms can be expressed in terms of the layer transports, based on the definitions

$$Q_1 \equiv Bh_1u_1, \qquad Q_2 \equiv Bh_2u_2 \qquad [11]$$

and layer Froude numbers

$$F_1^2 = \frac{Q_1^2}{g'B^2h_1^3}, \qquad F_2^2 = \frac{Q_2^2}{g'B^2h_2^3} \qquad [12]$$

These relations can be incorporated into the baroclinic momentum equation

$$\frac{1}{g'}\frac{\partial}{\partial t}(u_2 - u_1) + (1 - F_1^2 - F_2^2)\frac{\partial h_i}{\partial x} = -F_2^2\left(\frac{\partial h_b}{\partial x} \pm C_D\right) - \frac{F_1^2h_1 - F_2^2h_2}{B}\frac{\partial B}{\partial x} \pm C_iF_\Delta^2 + \frac{1}{g'}\left(\frac{u_2}{h_2} + \frac{u_1}{h_1}\right)\frac{\partial h_i}{\partial t} \qquad [13]$$

where the $\pm C_D$ term is positive for positive u_2 and negative for negative u_2, and the shear Froude number is defined by

$$F_\Delta^2 = \frac{(u_1 - u_2)^2}{g'h'}$$

where $h' = h_1h_2/(h_1 + h_2)$ and the sign of the $\pm C_i$ term is positive for $u_1 > u_2$.

This form of the momentum equation illustrates the importance of the composite Froude number

$$F_1^2 + F_2^2 = G^2 \qquad [14]$$

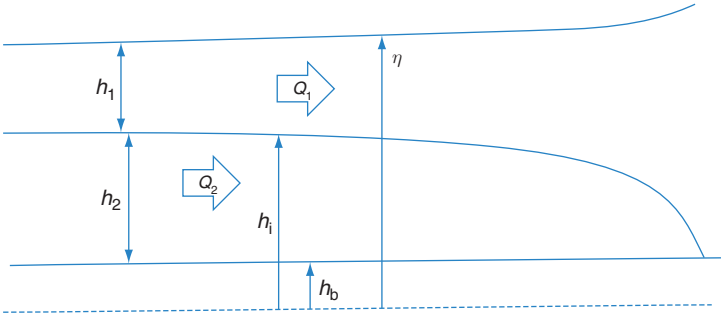

Figure 3 Schematic of a two-layer estuary.

as defined by Armi and Farmer (1986). The composite Froude number indicates whether the flow is subcritical or supercritical with respect to internal waves – for $G < 1$, long internal waves can travel in either direction, and for $G > 1$, waves can travel only in the downstream direction. Note that if the flow is traveling in the opposite direction in either layer, the downstream direction is determined by the layer with the larger layer Froude number – this is sometimes called the 'active' layer. The critical condition, or the condition for hydraulic control, is

$$G^2 = F_1^2 + F_2^2 = 1 \qquad [15]$$

The composite Froude number is one of the most important concepts in internal hydraulics and in the dynamics of highly stratified estuaries, as will be shown in the detailed examination of the dynamics that follows.

2.03.4 Salt Wedge Dynamics

The salt wedge regime occupies a small spot on the top of the Hansen–Rattray diagram, but research in the last 25 years has revealed that salt wedges are perhaps the most dynamic and variable of all estuarine systems, owing to the strong interaction among tidal, fluvial, and estuarine forcing. Salt wedges are not distinguished by the dominance of one particular forcing mechanism; rather, they can be characterized by the intensity of all of the forcing mechanisms. In the following subsections, different aspects of the dynamics relevant to salt wedges are discussed, based on extracting different terms from eqn [13] that are relevant to different situations, and then providing illustrations of these processes from observations.

2.03.4.1 Plume Lift-Off

A common situation within and at the mouths of two-layer estuaries is a hydraulic transition caused by a lateral expansion. Considering steady, inviscid flow through a contraction with flow confined to the upper layer, eqn [13] reduces to

$$\frac{\partial h_i}{\partial x} = -\frac{F_1^2}{1 - F_1^2}\frac{h_1}{B}\frac{\partial B}{\partial x} \qquad [16]$$

The structure of the lift-off regime for different strengths of outflow is shown in **Figure 4**, representing a highly stratified estuary through the course of the ebb tide. These different regimes were described by Armi and Farmer (1986) in context with flow over an obstacle, but they are also relevant to the conditions at the mouth of an estuary. Early in the ebb, the flow is subcritical in the estuary, but it transitions to supercritical at the mouth, with a thin plume spreading seaward (**Figure 4(b)**). As the ebb accelerates, the upper layer deepens in the estuary but remains subcritical, and a more pronounced hydraulic transition occurs at the mouth (**Figure 4(c)**). At some point, the outflow velocity exceeds the critical Froude number everywhere in the estuary, and a period of intense mixing ensues (see Section 2.03.4.4). This leads to the re-establishment of a frontal regime at the mouth, as shown in **Figure 4(d)**. The critical condition for the establishment of the front is that the upper layer occupies the entire water column, and $F_1 = 1$. The depth at which this occurs is

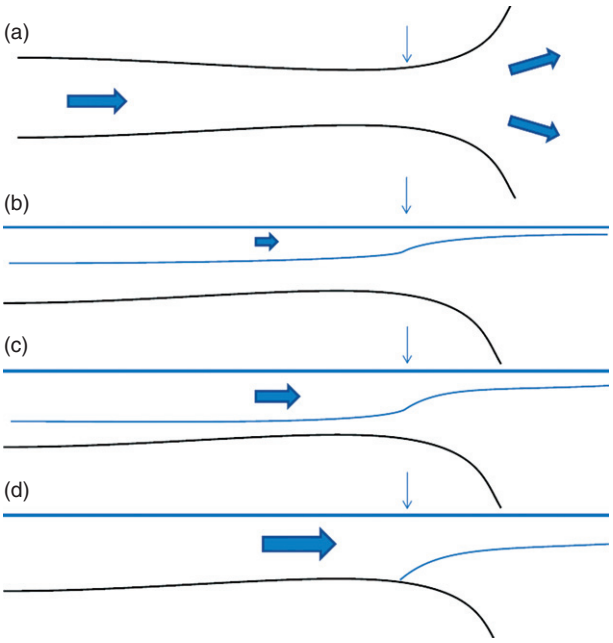

Figure 4 The plume lift-off regime for varying strength of outflow. (a) A plan view of the mouth of an estuary, with the minimum width indicated by the arrow. (b), (c), (d) The structure of the interface for varying strength outflow in the upper layer, with a stagnant lower layer. In the first two cases, the flow is subcritical within the estuary, but in the third case the outflow velocity exceeds the critical condition [17], and a front forms at the mouth.

$$h = h_{1C} = \left(\frac{Q_1^2}{B^2 g'}\right)^{1/3} \qquad [17]$$

This condition first occurs at the throat of the constriction, but as the ebb flow increases, the front moves seaward into deeper water and increased width B, thus maintaining the critical condition. Because the width and depth increase rapidly near the mouth, the front does not move very far seaward to maintain this critical condition near the mouth. The plume lift-off regime is seen at the mouth of the Fraser River (**Figure 5**, from MacDonald and Geyer (2005)). MacDonald and Geyer found that the analytical solution for the frontal position, eqn [17] was modified by three-dimensional (3D) geometry of the front. A critical Froude number remains the controling parameter, but the front occurred at an angle to the outflow with the frontal condition applying to flow normal to the front.

2.03.4.2 The Arrested Salt Wedge Regime

Schijf and Schonfeld (1953) as well as Stommel and Farmer (1952) worked out the equations for the arrested salt wedge, that is, a two-layer regime in which the lower layer is motionless, and the tilt of the interface balances a combination of advective acceleration of the upper layer and entrainment. In order to simplify the mathematics, the width and depth of the estuary are assumed to be constant. For this set of assumptions, eqn [13] simplifies to

$$\frac{\partial h_i}{\partial x} = \pm C_i \frac{F_1^2}{1 - F_1^2}\frac{h_0}{h_2} \qquad [18]$$

where $h_0 = h_1 + h_2$ and where the sign of the right-hand side is determined by the sign of u_1, that is, whether the estuary goes to

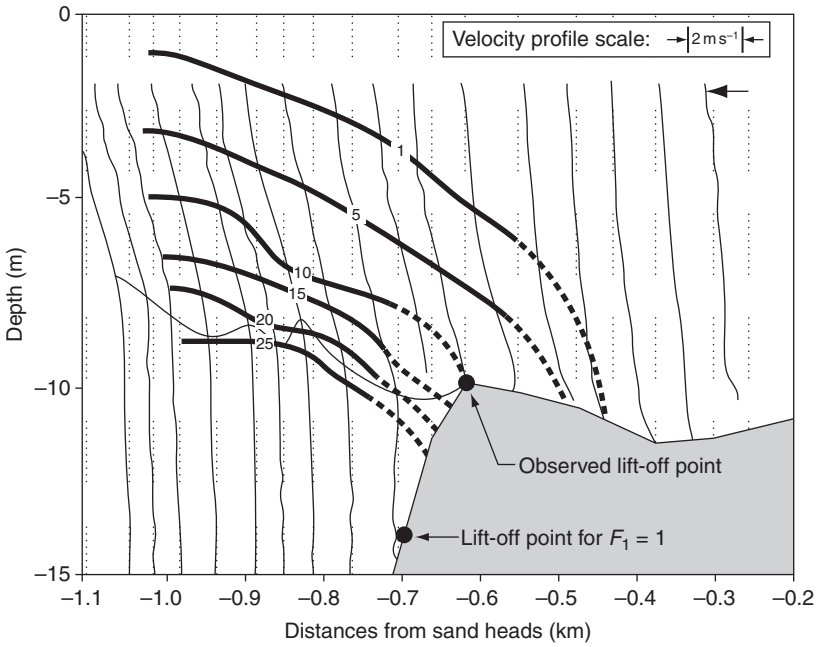

Figure 5 The plume lift-off front of the Fraser River. The authors found that the Froude number slightly exceeded the critical condition [17] in this case, due to three-dimensional effects. From MacDonald, D.G., Geyer, W.R., 2005. Hydraulic control of a highly stratified estuarine front. Journal of Physical Oceanography 35, 374–386.

the right or the left. Note that $\partial h_i/\partial x$ becomes infinite when $F_1 = 1$, that is, when the flow is critical, and when the lower layer vanishes. These two singularities define the landward and seaward ends of the domain. At the landward end, the interface intersects the bottom – the nose of the salt wedge, and at the seaward end the interface depth at the mouth is set by the critical condition [17] (although note that $h_{1c} < h_0$ in order for there to be a salt wedge. For stronger flows, the salt is expelled). Although eqn [18] cannot be solved analytically, it is a simple, first-order differential equation for the interface elevation that can be readily integrated numerically, with solutions as shown in **Figure 6**.

The solution only depends on one parameter, the freshwater Froude number

$$F_f = \frac{Q_f}{\left(\beta g s_0 B^2 h_0^3\right)^{1/2}} \qquad [19]$$

Note that F_f is the same as F_1 when the upper layer occupies the whole water column. The dependence of the salt wedge length on freshwater outflow (nondimensionalized as freshwater Froude number) is shown in **Figure 7**. The predicted length is compared with power-law relations $L \propto Q^{\alpha}$ where $\alpha = -2, -2.5$. These exponents are similar to those obtained by Keulegan (1957) in his empirical investigations of salt wedge intrusions. This is a much more sensitive dependence of length on discharge than is found in partially stratified estuaries, in which the value of α is around −0.2 to −0.3. The high sensitivity is related to hydraulic behavior of salt wedges. Note that the power law does not depend on the choice of C_i, although the length of the estuary is inversely proportional to its value. The actual value of C_i is difficult to determine *a priori*, because it depends on the details of the geometry and mixing processes within the estuary. A value around $(1-5) \times 10^{-4}$ is a reasonable gross estimate, based on the analysis of the Fraser River dynamics (Geyer, 1988).

This analysis is based on the assumption that the salt wedge is arrested, that is, that the salinity and velocity are in a steady-state regime. In the real world, there are few (if any) examples of salt wedge estuaries in which tidal processes do not result in significant time dependence of the salt wedge structure. Even in the Mississippi River, which is often cited as an arrested salt wedge, the influence of tides is quite pronounced, as shown by Wright (1971). The Ebro River estuary, which enters the Mediterranean Sea in Spain, is perhaps a better example than the Mississippi of a salt wedge minimally influenced by tides (Ibanez et al., 1997). The time dependence of the Ebro is due primarily to changes in river flow rather than tides.

Even in systems strongly influenced by tides, the Schijf and Schonfeld analysis is still useful for describing the quasi-steady structure of salt wedges during specific phases of the tidal cycle. Rather than considering the river flow in determining the value of F_1 in eqn [18], the sum of the river flow and tidal outflow should be considered. When the tidal discharge is accounted for, the solutions presented in **Figure 6** are consistent with the observed structure of the Fraser River salt wedge during the early ebb (e.g., **Figure 1(a)**; see Geyer and Farmer (1989) for a more detailed analysis.). At the point at which $F_1 > 1$, however, the solution is no longer valid, and rapid mixing of the salt wedge ensues (see Section 2.03.4.4).

2.03.4.3 The Advance of a Salt Wedge: The Influence of Bottom Friction

Bottom friction affects stratified flows if the horizontal scales are long relative to the frictional scale, that is, $C_D L/h_2 > 1$.

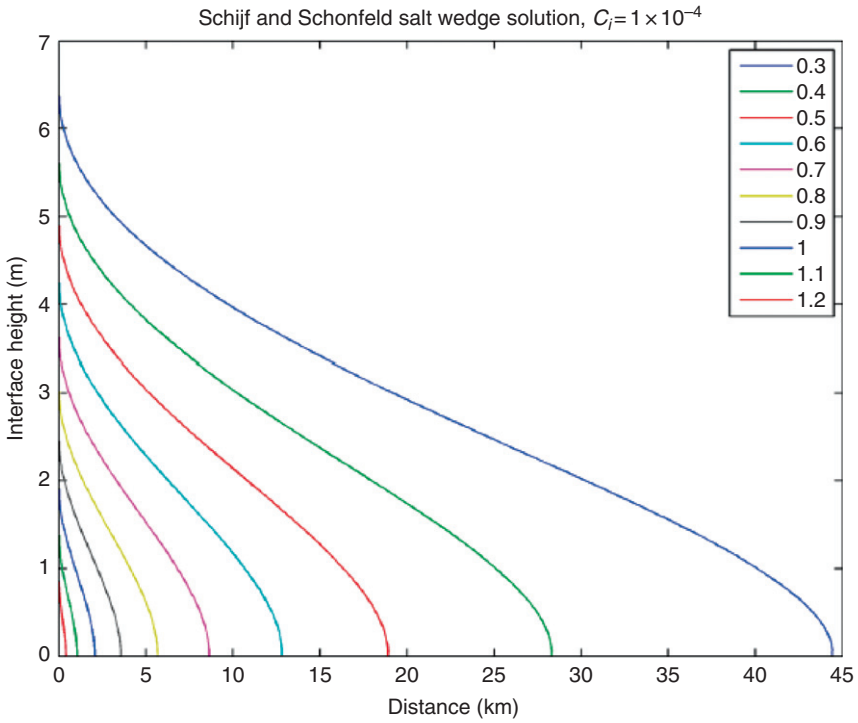

Figure 6 Schijf and Schonfeld (1953) solutions for the salt wedge equation [18]. For this example, the total depth $h_0 = 10$ m, $s_0 = 25$ psu, and $C_i = 10^{-4}$. Each of the curves represents a different freshwater outflow velocity, from 0.3 to 1.2 m s^{-1}.

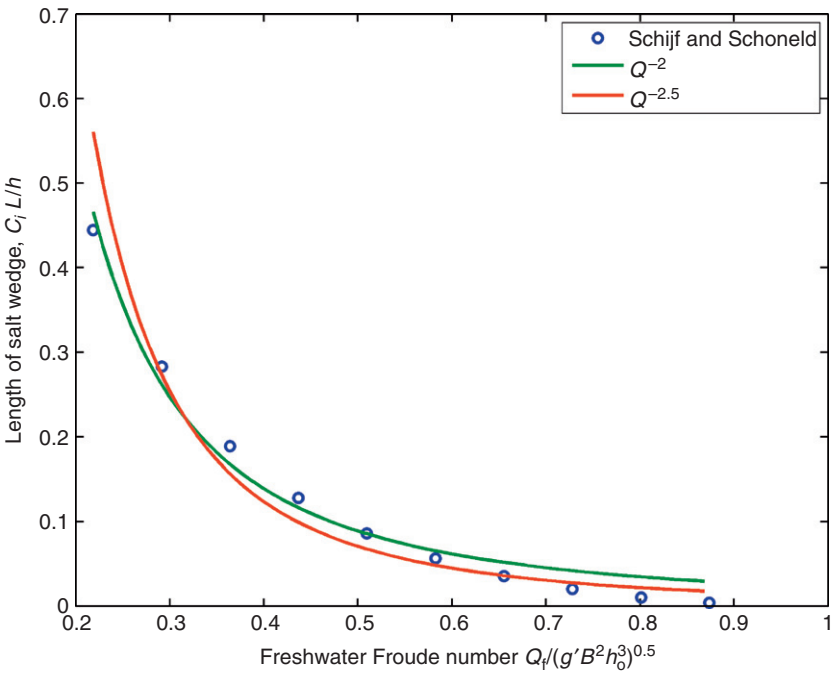

Figure 7 Length of Schijf and Schonfeld salt wedge L (nondimensionalized with depth and interfacial drag coefficient) as a function of freshwater Froude number (blue circles). Power-law curves of Q^{-2} and $Q^{-2.5}$ are shown for comparison.

One particularly simple but important illustration of the influence of friction is in the propagation of a salt wedge front during the flood tide in an estuary. If one considers a flat-bottomed estuary, with a salt wedge advancing into still water, the lower layer can be considered as a fixed shape translating up the estuary. In the reference frame moving with the advancing salt wedge, $\partial h_i/\partial t = 0$, and there is no along-estuary velocity gradient. If the accelerations of the upper layer are

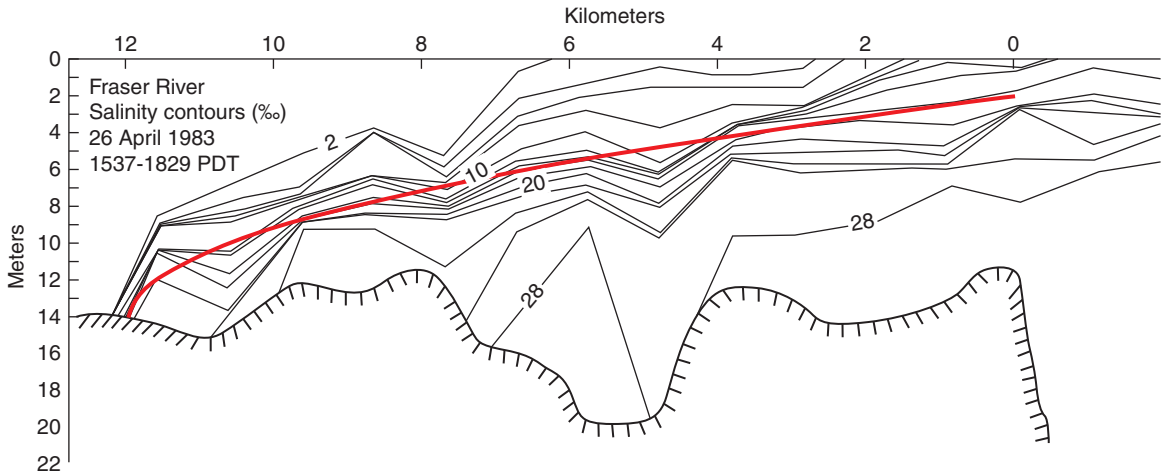

Figure 8 Salinity contours of the Fraser River during flood tide (from Geyer and Farmer, 1989), with the parabolic solution for salt wedge advance (eqn [21]) superimposed.

neglected (which is a good approximation for natural channels that widen significantly with height above the bottom), the momentum equation can be simplified to

$$\frac{\partial h_i}{\partial x} = -C_D F_2^2 \qquad [20]$$

Equation [20] can be integrated in x to obtain the height of the interface

$$h_i(x) = \left[\frac{2C_D u_2^2}{g'}\left(x_0 - x\right)\right]^{1/2} \qquad [21]$$

that is, the interface height forms a parabola, with its vertex at the nose of the salt wedge at $x = x_0$. The advancing salt wedge in the Fraser estuary provides an example of these dynamics, as shown in **Figure 8**. The Fraser advances at a rate of approximately $0.7\,\mathrm{m\,s^{-1}}$, with a bottom drag coefficient of about 3×10^{-3}. This very simple theory does a good job of reproducing the general shape of the salt wedge during the flooding tide, although the details are affected by the variability of estuary geometry as well as mixing and differential advection (see Geyer and Farmer (1989) for details).

2.03.4.4 Supercritical Estuarine Flow: Erosion of the Salt Wedge

The Schijf and Schonfeld salt-wedge regime requires subcritical flows, but as the strength of the ebb increases in a salt wedge, this constraint may be violated. Based on the Schijf and Schonfeld analysis as well as that of Armi (1985) and Armi and Farmer (1986), a steady two-layer regime cannot be maintained within the estuary with supercritical flow and thus the only steady solution is a front at the critical depth set by eqn [17]. However, there is a finite time in which there is still salt in the estuary, but the flow is supercritical. This is a period in which intense mixing is observed, as documented by Geyer and Smith (1987) and Geyer and Farmer (1989). These studies suggest that most of the mixing occurs in the pycnocline as a result of shear instability, but recent research in tidally varying salt wedges by Ralston et al. (2010) and Wang et al. (2009) indicates that shear instability in the pycnocline is the dominant mechanism for the initial breakdown of the salt wedge, but as the ebb progresses the mixing is driven by boundary-layer turbulence.

The occurrence of shear instability depends on the gradient Richardson number

$$Ri = -\frac{\left(\frac{g}{\rho}\right)\left(\frac{\partial \rho}{\partial z}\right)}{\left(\frac{\partial u}{\partial z}\right)^2} \qquad [22]$$

Instability can occur only if $Ri < 0.25$, as shown originally by Miles (1961). Several mechanisms contribute to increased shear, leading to conditions of $Ri < 0.25$ during the strong ebb flow. First of all, the near-bottom flow can no longer be arrested under supercritical conditions because the ebbing barotropic pressure gradient exceeds the baroclinic pressure gradient near the bed. Geyer and Farmer (1989) showed that supercritical conditions will lead to outflow of the near-bottom water and the generation of a bottom stress that augments the interfacial shear. Once this condition is reached, additional barotropic forcing (due to the combination of ebb tidal forcing and river outflow) will tend to augment the shear between the upper and lower layer. The other important mechanism is supercritical acceleration of the upper layer at topographic constrictions. Plume lift-off is one example, but hydraulic transitions can also occur due to topographic constrictions or sills within the estuary. These regions of supercritical acceleration cause both an increase of shear and a reduction of the vertical scale of the interface, causing Ri to decrease.

The increased lower layer shear and acceleration of the surface layer leads to spatially localized zones of intense shear instability. An echo sounder image from the Fraser River shows the thickening interface at several locations downstream of lateral constrictions, where the accelerating shear flow becomes unstable (**Figure 9**). A higher resolution image of shear instability in the Connecticut River details billows observed in a regime similar to the mixing zones of the Fraser River.

Shear instability is important during the initial breakdown of the salt wedge, but as the near-bottom flow accelerates in conjunction with the breakdown of the density structure, boundary-generated turbulence starts to dominate over shear

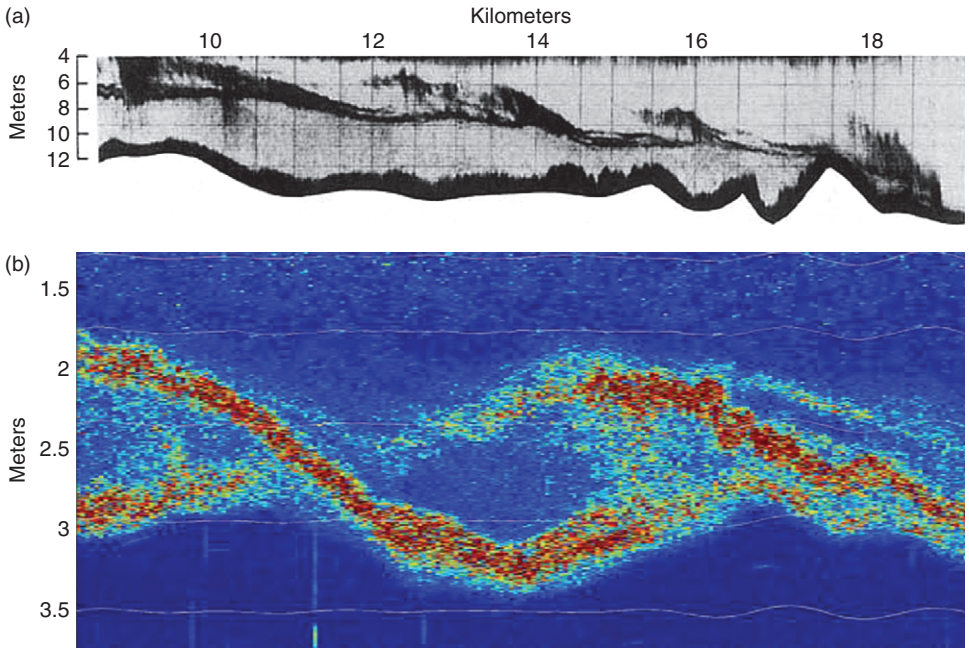

Figure 9 Shear instabilities observed by echo sounders. (a) Large-scale view of regions of shear instability in the Fraser estuary. (b) Close-up of shear instabilities in the Connecticut River (observations by the authors). The wavelength of the instabilities in the lower image is roughly 10 m. In both cases, the top-to-bottom salinity difference is 24–28 psu, and the velocity differences between the upper and lower layer are more than 1 m s^{-1}. (a) Geyer, W.R., Farmer, D.M., 1989. Tide induced variation of the dynamics of a salt wedge estuary. Journal of Physical Oceanography 28, 1060–1072.

instability. In fact, Ralston et al. (2010) indicated that more than half of the buoyancy flux associated with mixing during the ebb in the Merrimack River estuary occurs in the bottom boundary layer rather than in an elevated shear layer. They distinguished boundary mixing from shear mixing based on whether the maximum stress is found at the bottom or if there is a distinct maximum within the pycnocline. Once the stress maximum reaches the bottom, the mixing is consistent with the dynamics of stress-driven mixed layers, as described by Kato and Phillips (1969), Price et al. (1986), and Trowbridge (1992). Under these conditions, the mixing rate is found to scale with the intensity of the bottom stress.

2.03.5 Fjord Dynamics

Fjords act as strongly stratified estuaries due to their great depth and relatively weak tidal mixing. The potential energy of the water column depends quadratically on depth (eqn [6]), so deep, stratified fjords have a large amount of potential energy and thus weak vertical exchange. As a consequence, the exchange in fjords is dominated by horizontal transport processes. Vertical mixing does occur at sills, but it tends to be localized and the timescales of horizontal exchange tend to be shorter than the timescales of vertical mixing.

Owing to their large depth, the tidal exchange in fjords is small compared to their overall volume. In fact, the combination of limited vertical exchange and limited tidal exchange means that the residence times of fjords are relatively long, and gravitational (two-layer, density-driven) exchange flow is more important than tidal exchange. Much of the research in fjords has been directed at quantifying the exchange flow and determining its influence on fjord residence time and bottom-water renewal. The following sections address the kinematics and dynamics of exchange flow as they relate to fjord circulation.

2.03.5.1 Knudsen's Relation

Knudsen (1900) developed a set of equations to characterize the exchange flow in fjords and similar stratified basins, based on his analysis of the exchange processes in the Baltic Sea. The basin is assumed to be in steady state with respect to volume and salt, with a two-layer exchange flow at the mouth and river inflow. Volume conservation requires that

$$Q_f = Q_1 - Q_2 \qquad [23]$$

where Q_f is the river inflow, Q_1 is the volume outflow in the upper layer, and Q_2 is the inflow in the lower layer (**Figure 10**). The salt balance requires that

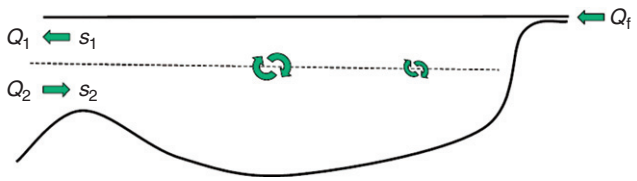

Figure 10 Schematic of a fjord, illustrating the variables included in Knudsen's relation.

$$Q_1 s_1 = Q_2 s_2 \quad [24]$$

where $s_1$and s_2 are layer-averaged salinities of the upper and lower layers at the mouth. Equations [23] and [24] can be combined to form the following relations for the magnitude of the exchange flow:

$$Q_1 = Q_f \frac{s_2}{s_2 - s_1} = PQ_f \quad [25a]$$

$$Q_2 = Q_f \frac{s_1}{s_2 - s_1} = (P - 1)Q_f \quad [25b]$$

where $P = s_2/(s_2 - s_1)$ is what Stigebrandt (1981) calls the 'mixing factor', the ratio of volume of brackish water outflow in the upper layer to the freshwater inflow. Knudsen's relation thus allows the net exchange flow to be readily determined based on knowledge of the salinity distribution and the freshwater inflow. Note that the requirement of a steady-state balance is typically not satisfied on timescales much shorter than the residence time of freshwater in the fjord; these equations apply to the time-average exchange flow. Also, Knudsen's relation assumes that the salt transport is accomplished only by the two-layer exchange flow, neglecting tidal dispersion and other time-dependent exchange processes. Notwithstanding these limitations, Knudsen's relation provides one of the most valuable diagnostics for exchange flows in stratified basins.

2.03.5.2 Hydraulic Control at the Fjord Mouth and Overmixing

Stommel and Farmer (1953) first developed the idea of hydraulic control in fjords to explain the exchange at the mouth. Stigebrandt (1981) provides a clear summary of these ideas and extends them to include the influence of mixing. The basic idea is that the flow is controlled at the mouth, that is, the composite Froude number (eqn [14]) $G^2 = 1$. For what Stigebrandt calls 'normal' or N fjords, the upper layer is much thinner than the lower layer and the control condition can be approximated as $F_1{}^2 = 1$. This constraint can be combined with Knudsen's relation to obtain expressions for the velocity and upper layer depth at the mouth of an N fjord:

$$h_{1M} = P\left(\frac{Q_f^2}{\beta g s_2 B^2}\right)^{1/3} \quad [26]$$

$$u_{1M} = \left(\frac{Q_f \beta g s_2}{B}\right)^{1/3} \quad [27]$$

where the subscript M refers to conditions at the mouth and B is the width.

Using the definition of the freshwater Froude number (eqn [19]), the velocity and interface depth at the mouth become

$$\frac{h_{1M}}{h_M} = PF_f^{2/3} \quad [28]$$

$$\frac{u_{1M}}{u_f} = \frac{1}{F_f^{2/3}} \quad [29]$$

where u_f is the freshwater velocity Q_f/Bh_M. Note that the velocity of the upper layer is invariant with mixing. As the mixing factor P increases, the volume flux Q_1 increases, but the layer depth increases in the same proportion (eqn [28]), yielding the same velocity. Solutions to eqns [28] and [29] for different values of mixing parameter and freshwater Froude number are shown in **Figure 11**. Note that for small values of F_f, the upper-layer outflow is much higher than the river outflow, but as F_f approaches 1, the speed-up decreases and the layer thickness increases. Note also the joint dependence of the layer thickness on F_f and the mixing parameter P.

As mixing increases as freshwater outflow increases, there comes a point at which the composite Froude number

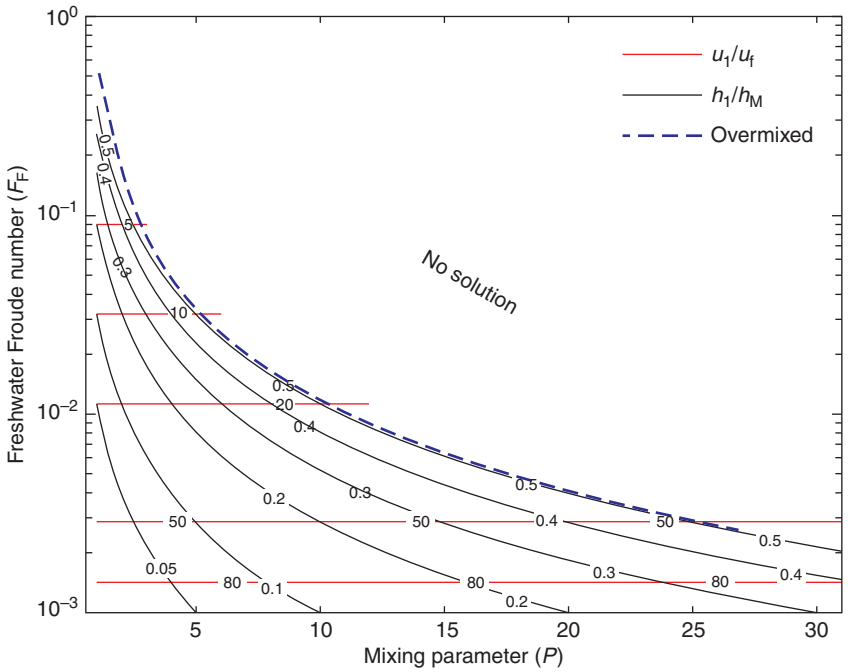

Figure 11 Upper layer velocity ratio u_1/u_f and nondimensional thickness h_1/h_M for N fjords, based on eqns [28] and [29]. The dashed line indicates the over-mixed limit, that is, O fjords. The upper part of the curve violates the Froude number constraint for exchange flow.

$G^2 > 1$. For small values of F_f, this occurs close to the point where $h_{1M}/h_M = 1/2$. As F_f approaches 1, the critical depth approaches the entire water depth. This is called the 'over-mixing limit' (Stommel and Farmer, 1953), or the 'O' fjord (Stigebrandt, 1981), shown as a dashed line on Figure 11. Above this line, exchange flow is not possible, because $G^2 > 1$ for all values of h_{1M}/h_M.

Overmixing is a challenging and somewhat nonintuitive concept. It is best understood by considering a fjord with constant inflow F_f that starts with weak mixing, so it is below the overmixing limit. As the mixing increases, the layer depth increases (moving horizontally in Figure 11), until the layer depth reaches roughly half of the water depth. If mixing continues beyond this point, the flow becomes supercritical, and the exchange flow will decrease, due both to changes in the momentum balance and to mixing of momentum in the control section. This reduction in exchange flow, combined with a reduction in salinity difference between the layers, will cause a reduction in the salt flux into the fjord, or a choked condition. Knudsen's relation will no longer be satisfied, that is, the salt balance will become time dependent. The salinity in the fjord will decrease until the salinity difference becomes large enough to re-establish hydraulic control.

This scenario leads to the paradoxical conclusion that the maximum amount of mixing that can occur in a fjord does not depend on the actual mixing mechanisms, but rather on the geometry of the mouth and the freshwater inflow. This paradox is resolved by the transient response of the salinity distribution within the fjord to choked conditions. This adjustment will continue (even in the presence of intense mixing) until the salinity gradients are distributed in such a way as to re-establish hydraulic control. In most fjords, the mixing events and freshwater inflow are episodic, while the salt balance represents the average condition over the residence time of freshwater in the fjord, which could be weeks to months. Nevertheless, the overmixing constraint provides an important framework for addressing the mean conditions in a fjord and particularly how it may respond to changes in forcing conditions.

2.03.5.3 Hydraulics of Flow Over Sills

Flows over sills in fjords provide some of the best natural applications of two-layer hydraulics. If we consider a steady flow with uniform width and no friction, the momentum eqn [13] reduces to

$$\partial \frac{h_i}{\partial x} = \frac{-F_2^2}{1-G^2} \frac{\partial h_b}{\partial x} \qquad [30]$$

For subcritical flow ($G < 1$), the response of the interface is opposite that of changes in bottom elevation (**Figure 12(a)**), but the interface follows the bottom for $G > 1$ (**Figure 12(b)**). Note that the equation is singular for $G = 1$. The only steady solution for $G = 1$ is the case in which $\partial h_b/\partial x = 0$. This is the familiar hydraulic transition at the crest of an obstacle, analogous to the flow over a weir in single-layer hydraulics (**Figure 12(c)**).

A dramatic example of hydraulic response at a sill is at Knight Inlet, where an echo-sounding image of the density interface captures the transition to supercritical conditions followed by a downstream jump to subcritical flow (Farmer and Armi, 1989). Hydraulic jumps provide an important source of mixing in estuaries, as discussed by a number of authors including Partch and Smith (1978), Farmer and Smith (1980), Seim and Gregg (1994), Farmer and Armi (1999), and Klymak and Gregg (2004). A word of caution – eqn [15] does not consider the influence of friction. If the bottom slope is comparable or smaller than the bottom drag coefficient, that is, $C_D > |\partial h_b/\partial x|$, then frictional effects are more important than bottom topography (eqn [13]). The scaling for this relationship is $C_D L/h_2 > 1$ (where L is the horizontal scale of the topography) for bottom friction to dominate the dynamics. For representative values of $C_D = 0.0002$ and $h_2 = 50$ m (e.g., a fjord), advective processes dominate over friction up to scales of 25 km. For a shallow estuary with $h_2 = 5$ m (e.g., a salt wedge estuary), bottom friction will dominate over bottom topography at scales greater than 2.5 km except during periods such as the early ebb in which near-bottom flows are weak.

2.03.5.4 Deep-Water Renewal

In many deep fjords with sills, the two-layer circulation described by Knudsen's relation applies to the flow above the sill level, but there is a deeper layer that is generally out of contact with this estuarine circulation. The flushing of the deep water is often much slower than the exchange of the upper water column, and the deep water may become hypoxic or even anoxic as a result. The mechanisms responsible for deep-water renewal are thus important in consideration of fjord water quality. A variety of mechanisms may result in deep water renewal, including spring–neap variability of tidal conditions at the sill (Edwards and Edelsten, 1977; Geyer and Cannon, 1982), seasonal variability of the density of the adjacent oceanic water (Cannon et al., 1990), and meteorological forcing (Skreslet and Loeng, 1977). The mechanisms of renewal involve an interesting combination of time-dependent hydraulics and gravity current dynamics.

2.03.5.5 Mixing in Fjords

The dramatic echo sounding image by Farmer and Armi (**Figure 13**) illustrates the importance of sills for mixing in fjords. This image shows shear instabilities at the crest of the obstacle and mixing in the hydraulic jump region downstream. The higher velocities in the vicinity of sills combined with the enhanced shears associated with hydraulic transitions lead to conditions favorable for mixing. A number of studies have investigated the mechanisms and consequences of mixing at sills, including Ebbesmeyer and Barnes (1980), Geyer and Cannon (1982), and Seim and Gregg (1997).

Winds provide another important source of mixing in fjords. Stigebrandt (1981) balanced the energy input by winds with the work required to entrain dense water into the upper layer, obtaining an expression for the mixing parameter P:

$$P = 1 + \frac{\Psi u_*^3 A}{Q_f g' h_1} \qquad [31]$$

where u^* is the friction velocity associated with the wind, Ψ is an $O(1)$ constant involving the mixing efficiency and the surface drag coefficient. This expression is similar to the inverse of the estuarine Richardson number (eqn [4]), which parametrizes the

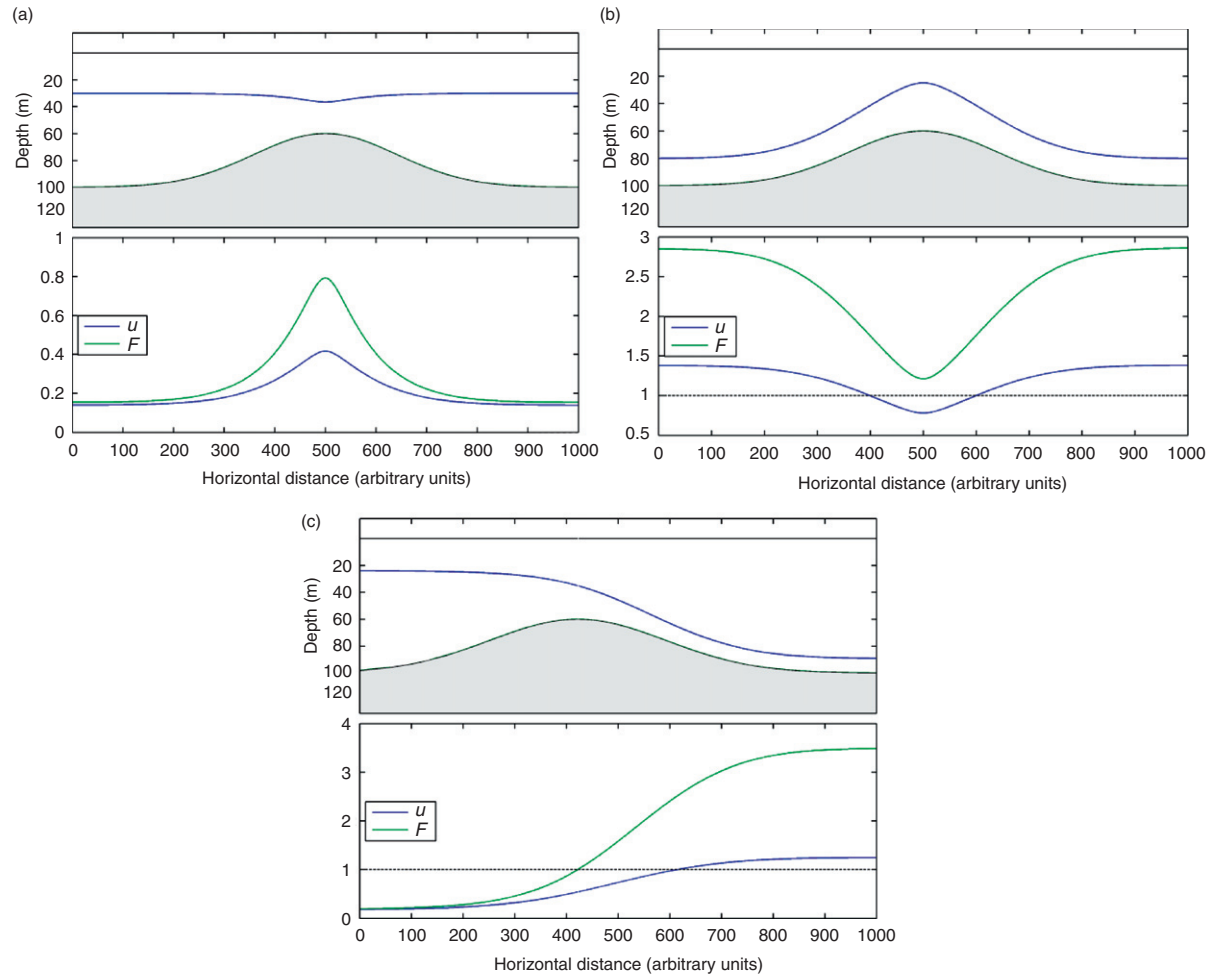

Figure 12 Two-layer flow over a bump, with flow only in the lower layer, and $\Delta s = 1.5$ psu. Velocity is in m s^{-1}: (a) subcritical flow; (b) supercritical flow; (c) transition from subcritical to supercritical. Note that in the subcritical case, the flow accelerates over the bump, but in the supercritical case it decelerates. In the hydraulic transition, the flow accelerates both on the upstream and downstream sides of the bump. Typically, the flow will jump back to subcritical somewhere on the downstream side of the bump.

influence of tidal mixing on estuarine stratification, but with wind as the source of mixing energy rather than the tides. Stigebrandt uses this relation in combination with the internal hydraulics to derive solutions for the layer thickness as a function of wind stress and freshwater flow, with results for Nordfjord shown in **Figure 14**. This graph indicates that the upper layer thickness depends strongly on wind speed irrespective of river discharge, varying from around 1 m for calm conditions to more than 10 m for winds of 10 m s^{-1}. An interesting characteristic of the solution is that for low wind speeds, the upper layer thickness is greater for higher river outflows (consistent with the hydraulic constraint of eqn [28]), but for strong winds, the upper layer is thinner for stronger outflow rates (consistent with the stabilizing influence of buoyancy indicated in eqn [31]).

2.03.6 Unresolved Questions and Prospects for Future Research

This chapter provides only a brief survey of the state of the knowledge of strongly stratified estuaries. The reader will find a much richer and more interesting experience of the dynamics of these estuaries by pursuing the original literature. In the interest of providing background, some of the innovative new results have not been included here. In particular, numerical models have recently reached the level of sophistication that they can resolve complex interactions between the topographically forced flow and stratified mixing processes (e.g., Ralston et al., 2010; Wang et al., 2009). Numerical models of estuaries still need to parametrize vertical mixing processes, and although we are gaining confidence in turbulence closure formulations, there still remain questions about the accuracy of the parametrization of stratified mixing, particularly in regions of abrupt changes in topography.

An area of particular promise for future research in highly stratified estuaries is the investigation of small-scale topographic variability and its influence on the overall estuarine dynamics, either through mixing or through advective transport of momentum and mass. Farmer and Armi's image of the hydraulic transition in Knight Inlet (**Figure 13**) serves as a reminder of the interaction of processes at different scales that impact the estuarine-scale processes. Models are now approaching the resolution and accuracy at which the interactions of tidal flow with topography, internal

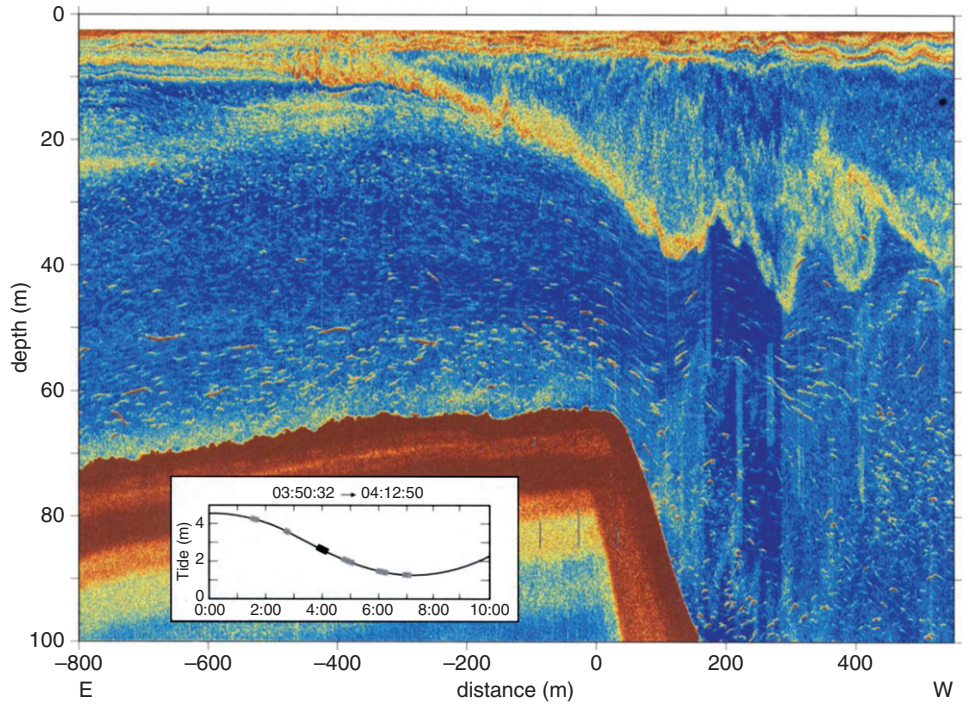

Figure 13 A hydraulic transition over the sill at Knight Inlet, with subcritical flow coming from the left and transitioning to supercritical at the sill crest. The flow jumps back to subcritical downstream of the sill crest at approximately 200 m. From Farmer and Armi (1989).

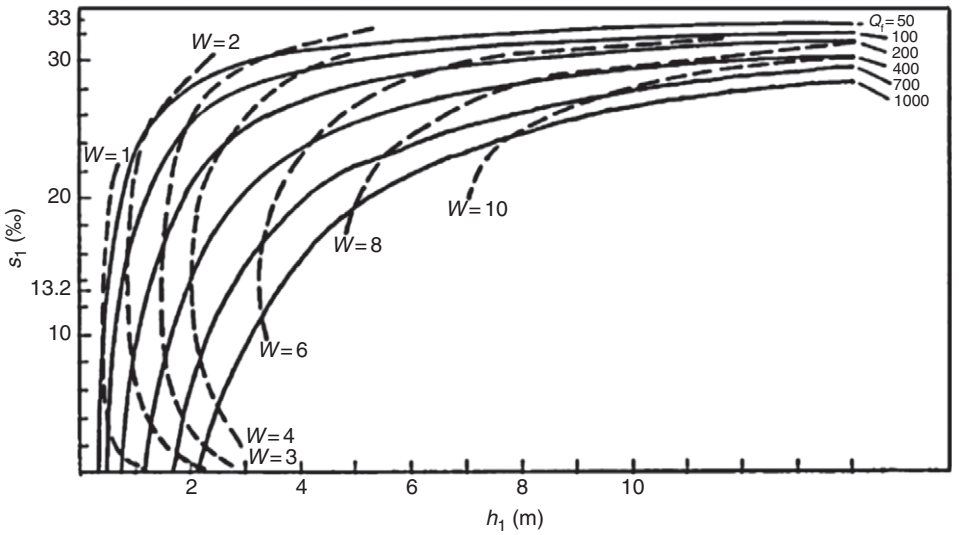

Figure 14 Influence of wind (W, in m s^{-1}) and river discharge (Q_f, in m^3 s^{-1}) on upper layer salinity and layer thickness in the Nordfjord, from Stigebrandt (1981). The layer thickness increases and the upper layer salinity increases strongly as the wind speed increases. Note that for weak winds, the upper layer thickness increases with river discharge (due to the Froude number effect), whereas for strong winds, the upper layer is thinner for higher discharge rates (due to the stabilizing influence of buoyancy relative to wind mixing).

hydraulics, secondary flows, shear instability, and turbulence can all be resolved. Moreover, our ability to measure the 3D structure continues to improve, both with *in situ* turbulence-resolving instruments and with remote acoustic techniques. The combination of sophisticated models and advanced observational approaches should lead to rapid progress in our quantification of the sub-mesoscale dynamics of strongly stratified estuaries.

Another area in which we can expect major breakthroughs is in our understanding of how physical processes affect ecological and biogeochemical processes in strongly stratified estuaries, particularly in the context of the response of the coastal environment to climate change. Strongly stratified estuaries are leading indicators of the effects of human stresses on the coastal environment. Stratification enhances the trapping of terrigenous wastes and organic matter, resulting

in eutrophication, hypoxia, and contaminant accumulation. The mechanisms of flushing and vertical mixing in strongly stratified estuaries are not just academic exercises – they have important consequences for environmental management and public health. Basic research into the physical mechanisms and their interactions with biogeochemical processes will provide the underpinnings for effective management of these important and vulnerable environments in the coming decades.

References

Armi, L., 1985. The hydraulics of two flowing layers with different densities. Journal of Fluid Mechanics 163, 27–58.

Armi, L., Farmer, D., 1986. Maximal two-layer exchange flow through a contraction with barotropic net flow. Journal of Fluid Mechanics 164, 27–51.

Bowen, M.M., 2000. Mechanisms and Variability of Salt Transport in Partially Stratified Estuaries. Ph.D. Thesis, Massachusetts Institution of Technology, Woods Hole Oceanographic Institution, Joint Program.

Cannon, G.A., Holbrook, J.R., Pashinki, D.J., 1990. Variations in the onset of bottom-water intrusions over the entrance sill of a fjord. Estuaries 3, 31–42.

Chatwin, P.C., 1976. Some remarks on the maintenance of the salinity distribution in estuaries. Estuarine and Coastal Marine Science 4, 555–566.

Dekshenieks, M.M., Donaghay, P.L., Sullivan, J.M., Rines, J.E.B., Osborn, T.R., Twardowski, M.S., 2001. Temporal and spatial occurrence of thin phytoplankton layers in relation to physical processes. Marine Ecology Progress Series 223, 61–71.

Ebbesmeyer, C.C., Barnes, C.A., 1980. Control of a fjord basin's dynamics by tidal mixing in embracing sill zones. Estuarine and Coastal Marine Science 11, 311–330.

Edwards, A., Edelsten, D.J., 1977. Deep water renewal of Loch Etive: a three basin Scottish Fjord. Estuarine and Coastal Marine Science 5, 575–595.

Farmer, D., Armi, L., 1989. Stratified flow over topography: the role of small-scale entrainment and mixing in flow establisnment. Proceedings of the Royal Society 455, 3221–3258.

Farmer, D.F., Armi, L., 1999. Stratified flow over topography: the role of small scale entrainment and mixing in flow establishment. Proceedings of the Royal Society of London 455A, 3221–3258.

Farmer, D.F., Smith, J.D., 1980. Tidal interaction of stratified flow with a sill in Knight Inlet. Deep-Sea Research 27A, 239–254.

Fischer, H.B., 1972. Mass transport mechanisms in partially stratified estuaries. Journal of Fluid Mechanics 53, 671–687.

Geyer, W.R., 1988. The advance of a salt wedge front: observations and dynamical model. In: Dronkers, J., van Leussen, W. (Eds.), Physical Processes in Estuaries. Springer, New York, NY, pp. 181–195.

Geyer, W.R., Cannon, G.A., 1982. Sill processes related to deep water renewal in a fjord. Journal of Geophysical Research 87, 7985–7996.

Geyer, W.R., Farmer, D.M., 1989. Tide induced variation of the dynamics of a salt wedge estuary. Journal of Physical Oceanography 28, 1060–1072.

Geyer, W.R., Smith, J.D., 1987. Shear instability in a highly stratified estuary. Journal of Physical Oceanography 17, 1668–1679.

Hansen, D.V., Rattray, M., Jr., 1966. New dimensions in estuary classification. Limnology and Oceanography 11, 319–326.

Ibanez, C., Pont, D., Prat, N., 1997. Characterization of the Ebro and Rhone estuaries: a basis for defining and classifying salt-wedge estuaries. Limnology and Oceanography 42, 89–101.

Kato, H., Phillips, O.M., 1969. On the penetration of a turbulent layer into stratified fluid. Journal of Fluid Mechanics 37, 643–655.

Keulegan, G., 1957. Eleventh progress report on model laws for density currents: form characteristics of arrested saline wedges. National Bureau of Standards Report 5482.

Klymak, J.M., Gregg, M.C., 2004. Tidally generated turbulence over Knight Inlet sill. Journal of Physical Oceanography 34, 1135–1151.

Knudsen, M., 1900. Ein hydrographischer Lehrsatz. Annalen der Hydrographie und Maritimen Meteorologie 28, 316–320.

MacDonald, D.G., Geyer, W.R., 2004. Turbulent energy production and entrainment at a highly stratified estuarine front. Journal of Geophysical Research 109, doi:10.1029/2003JC002094.

MacDonald, D.G., Geyer, W.R., 2005. Hydraulic control of a highly stratified estuarine front. Journal of Physical Oceanography 35, 374–386.

Miles, J.W., 1961. On the stability of heterogeneous shear flows. Journal of Fluid Mechanics 10, 496–508.

Partch, E.N., Smith, J.D., 1978. Time dependent mixing in a salt wedge estuary. Estuarine and Coastal Marine Science 6, 3–19.

Price, J.F., Weller, R.A., Pinkel, R., 1986. Diurnal cycling: observations and models of the upper ocean response to diurnal heating, cooling and wind mixing. Journal of Geophysical Research 91, 8411–8427.

Ralston, D.K., Geyer, W.R., Lerczak, J.A., 2010. Structure, variability and salt flux in a strongly forced estuary. Journal of Geophysical Research 115, 21.

Schijf, J.B., Schonfeld, J.C., 1953. Theoretical considerations on the motion of salt and fresh water. Proceedings of the Minnesota International Hydraulics Convention, 5th Congress I.A.H.R., pp. 321–333.

Schultz, E.A., Simmons, H.B., 1957. Fresh water–salt water density currents, a major cause of siltation in estuaries, Technical Bulletin No. 2. Committee on Tidal Hydraulics, U.S. Army Corps of Engineers, 28 pp.

Seim, H.E., Gregg, M.C., 1994. Detailed observation of a naturally occurring shear instability. Journal of Geophysical Research 99, 10049–10073.

Seim, H.E., Gregg, M.C., 1997. The importance of aspiration and channel curvature in producing strong vertical mixing over a sill. Journal of Geophysical Research 102, 3451–3472.

Simpson, J.H., Brown, J., Matthews, J., Allen, G., 1990. Tidal straining, density currents, and stirring in the control of estuarine stratification. Estuaries 13, 125–132.

Skreslet, S., Loeng, H., 1977. Deep water renewal and associated processes in Skjomen, a fjord in north Norway. Estuarine and Coastal Marine Science 5, 383–398.

Stacey, M.T., Burau, J.R., Monismith, S.G., 2001. Creation of residual flows in a partially stratified estuary. Journal of Geophysical Research 106, 17013–17037.

Stigebrandt, A., 1981. A mechanism governing the estuarine circulation in deep, strongly stratified fjords. Estuarine, Coastal and Shelf Science 13, 197–211.

Stommel, H., Farmer, H.G., 1952. On the nature of estuarine circulation. Woods Hole Oceanographic Institute. Technical Report Ref 52-88.

Stommel, H., Farmer, H.G., 1953. Control of salinity in an estuary by a transition. Journal of Marine Research 12, 13–20.

Trowbridge, J.H., 1992. A simple description of the deepening and structure of a stably stratified flow driven by a surface stress. Journal of Geophysical Research 97, 15529–15543.

Wang, B., Fringer, O.B., Giddings, S.N., Fong, D.A., 2009. High-resolution simulation of a macrotidal estuary using SUNTANS. Ocean Modelling 28, 167–192.

Wright, L.D., 1971. Hydrography of South Pass, Mississippi River. Journal of the Waterways, Harbors and Coastal Engineering Division 97, 491–504.